A Numerical Method for Calibrating Microwave Cavities for Plasma Diagnostics—Part I[1]

MICHAEL E. FEIN, MEMBER, IEEE, LAVVERNE A. SCHLIE, MEMBER, IEEE, JOSEPH T. VERDEYEN, MEMBER, IEEE, AND BLAKE E. CHERRINGTON, MEMBER, IEEE

Abstract—**Computer programs are described which generate calibration curves for TE_{0np} and TM_{0n0} cylindrical microwave cavities used in plasma diagnostics. The programs provide data for electron densities well above those at which perturbation theory fails, and can be used for any specified variation of electron density with radius.**

I. Introduction

IT HAS BECOME commonplace to measure electron number density and collision frequency in a plasma by observing the effect of the plasma on the resonant frequency and Q of a cylindrical microwave cavity. This technique was first reported by Brown *et al.* [1]–[3] and has since been extended by many authors. We refer to just two of the most recent works [4], [5] whose bibliographies provide an entry to the earlier literature, and to one particularly lucid elementary introduction to the method [6].

It is the purpose of this paper to describe computer programs of broad applicability to allow those who are interested in applying this valuable diagnostic technique to accurately calibrate their cavities without spending undue time developing their own programs. Part II of this paper presents complete tested computer programs for this purpose.

The simplest way to generate a calibration curve for a microwave cavity, and for that reason probably the one most often used, is Brown's original method—perturbation theory. A disadvantage of perturbation theory, however, is that it is valid only for relatively small frequencies (say $\omega_p < \omega$ for TM_{010} cavities, or $\omega_p < 10\omega$ for TE_{011} cavities). The literature contains the results of many numerical calculations and special-case analytic solutions designed to produce curves valid at higher densities; of late, these solutions have become increasingly general in their range of applicability [4], [5].

In this paper we wish to illustrate that for cylindrical plasmas whose only density variation is radial, in the absence of any magnetic field, the simple method of expanding the electric field within the plasma in a power series leads to relatively fast computer generation of calibration curves for TE_{0np} and TM_{mn0} cavity modes for almost any physically realizable radial density distribution.

Although this method should be applicable to a variety of cylindrically symmetric geometries, we have chosen to analyze the one particularly common arrangement (see Fig. 1). For this case, we present tested computer programs in Part II so that the method can be used without several man-months of preparation. The programs are written in the widely available Fortran IV language, and are documented thoroughly enough to make further development by the user a possibility.

The following restrictions must be taken into account.

1) Cavity Q and collision frequency are neglected in the analysis, although a straightforward method of dealing with them is suggested.

2) We do not explicitly calculate the effects of the large holes in the cavity where the plasma tube enters. This should cause errors of under 10 percent in the TM_{010} mode if the ratio of cavity length to plasma radius exceeds four [7], and should be still less serious for TE modes, whose E-fields do not terminate on end walls and which are, in any event, weak near those walls.

3) We present programs to deal only with the TE_{0np} and TM_{0n0} modes; extension of the TM program to the more general TM_{mn0} case should be merely time-consuming, not difficult.

4) The programs are written to handle only densities up to $(\omega_p^2/\omega_0^2) = 1000$. This restriction can be eliminated by changing one card in each program, but at an increased risk of finding spurious solutions.

5) The largest mode order accepted is 20. This restriction could be removed, if there were ever reason, by some attention to scaling of parameters to avoid computer overflow.

II. Mathematical Development

We begin with the inhomogeneous time-independent wave equation,

$$\nabla(\nabla \cdot E) - \nabla^2 E = \frac{\omega^2}{c^2} n^2 E \tag{1}$$

where n is the refractive index. For simplicity, we wish to decouple the vector equation, (1), so as to obtain a

Manuscript received November 5, 1970; revised September 1, 1971. This work was supported by the Aerospace Research Laboratory, OAR, Wright-Patterson Air Force Base, Ohio, under Contract AF 33(615)-5248.

The authors are with the Gaseous Electronics Laboratory, Department of Electrical Engineering, University of Illinois, Urbana, Ill. 61801.

[1] "A numerical method for calibrating microwave cavities for plasma diagnostics—Part II," this issue, p. 83.

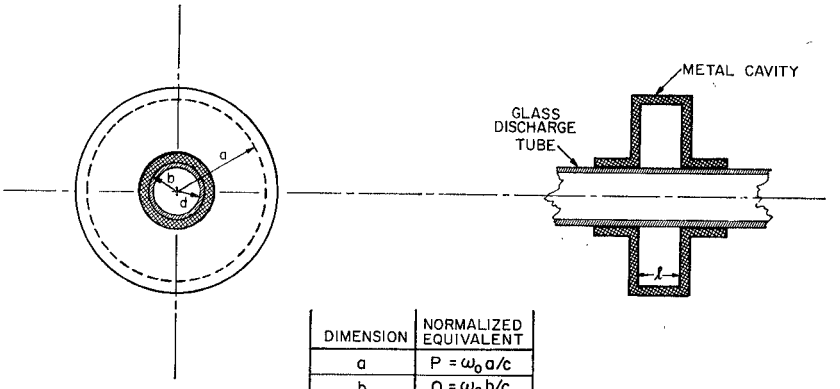

DIMENSION	NORMALIZED EQUIVALENT
a	$P = \omega_0 a/c$
b	$Q = \omega_0 b/c$
d	$R = \omega_0 d/c$
ℓ	$S = \omega_0 \ell/c$

Fig. 1. Cavity geometry.

scalar equation in one component of $\boldsymbol{E}$. We use Maxwell's equation for $\nabla \times \boldsymbol{H}$ to write

$$0 \equiv \nabla \cdot (\nabla \times \boldsymbol{H}) = j\omega\epsilon_0(\boldsymbol{E} \cdot \nabla n^2 + n^2 \nabla \cdot \boldsymbol{E}). \tag{2}$$

If we now restrict ourselves to cavity modes having no radial E-field component (TE_{0np} or TM_{mn0}) and require that the only gradients in n^2 be radial, (2) indicates that $\nabla \cdot E = 0$. Then (1) simplifies to the time-independent Helmholtz equation

$$\nabla^2 \boldsymbol{E} + \frac{\omega^2}{c^2} n^2 \boldsymbol{E} = 0. \tag{3}$$

For TE_{0np} modes in cylindrical cavities, we anticipate

$$\boldsymbol{E} = \hat{r}0 + \hat{\phi} E(r) \sin \frac{p\pi z}{l} + \hat{z}0. \tag{4}$$

Then, using the vector Laplacian in cylindrical coordinates [8], (3) becomes

$$\frac{d^2E}{dr^2} + \frac{1}{r}\frac{dE}{dr} + \left[\frac{\omega^2}{c^2} n^2 - \frac{p^2\pi^2}{l^2} - \frac{1}{r^2}\right] E = 0. \tag{5}$$

We normalize this equation by measuring all lengths in terms of the free-space wavelength λ_0 of the unperturbed cavity resonance ω_0.

$$x \equiv \frac{\omega_0}{c} r \equiv \frac{2\pi}{\lambda_0} r. \tag{6}$$

The dimensions of the cavity under discussion, and their normalized equivalents, are shown in Fig. 1. We also define a normalized frequency as

$$W \equiv \frac{\omega}{\omega_0}. \tag{7}$$

The normalized equivalent of (5) is

$$\frac{d^2E}{dx^2} + \frac{1}{x}\frac{dE}{dx} + \left[W^2 n^2 - \frac{p^2\pi^2}{S^2} - \frac{1}{x^2}\right] E = 0. \tag{8}$$

Once (8) has been solved for E, we may obtain H_z from curl $\boldsymbol{E} = -\dot{\boldsymbol{B}}$, which leads to

$$H_z = -\frac{1}{jW\eta_0}\frac{1}{x}\frac{d(xE)}{dx} \tag{9}$$

where $\eta = \sqrt{\mu_0/\epsilon_0}$. ($H_r$ exists but is not needed in the calculation.) We begin by solving (8) in the outer annulus, $Q \leq x \leq P$, subject to the boundary condition $E = 0$ at the outer wall, $x = P$. In this region, $n^2 = 1$, and (8) has the well-known solution

$$E(x) = A[J_1(h_0 x) - c_1 Y_1(h_0 x)] \tag{10}$$

where

$$c_1 = \frac{J_1(h_0 P)}{Y_1(h_0 P)} \tag{11}$$

and

$$h_0^2 = W^2 - \frac{p^2\pi^2}{S^2}. \tag{12}$$

Then (9) gives

$$H(x) = -\frac{Ah_0}{jW\eta_0}[J_0(h_0 x) - c_1 Y_0(h_0 x)]. \tag{13}$$

In the region occupied by the glass tube, $R \leq x \leq Q$, the fields are again a linear combination of J_1 and Y_1, but the refractive index of n_g alters the arguments of the Bessel functions. As a boundary condition, we require that the ratio of E to H at the glass–air interface $x = Q$ match the ratio obtained from (10) and (13). The result is

$$E = F[J_1(h_3 x) + c_3 Y_1(h_3 x)] \tag{14}$$

$$H = -\frac{h_3 F}{jW\eta_0}[J_0(h_3 x) + c_3 Y_0(h_3 x)] \tag{15}$$

where

$$c_3 \triangleq \frac{c_2 J_0(h_3 Q) - J_1(h_3 Q)}{Y_1(h_3 Q) - c_2 Y_0(h_3 Q)} \tag{16}$$

and

$$c_2 \triangleq \frac{h_3}{h_0}\frac{J_1(h_0Q) - c_1Y_1(h_0Q)}{J_0(h_0Q) - c_1Y_1(h_0Q)}. \tag{17}$$

We next solve for the fields in the plasma $x \leq R$. In this region, the refractive index is related to the plasma frequency

$$n^2 = 1 - W_p^2 \tag{18}$$

where

$$W_p^2 \equiv \frac{\omega_p^2}{\omega_0^2} = \frac{1}{\omega_0^2}\left(\frac{n_e q_e^2}{m_e \epsilon_0}\right). \tag{19}$$

In the plasma-filled region, (8) becomes

$$\frac{d^2E}{dx^2} + \frac{1}{x}\frac{dE}{dx} + \left[h_0^2 - W_p^2 - \frac{1}{x^2}\right]E = 0. \tag{20}$$

We now assume that the radial distribution of electrons in the tube is given by an arbitrary *even* power series, d_m, whose coefficients are to be provided by the experimenter.

$$W_p^2 = W_{p\text{-axial}}^2 \sum_{m=0}^{\infty} d_m \left(\frac{x}{R}\right)^{2m}, \qquad d_0 = 1. \tag{21}$$

For convenience in programming, we also define a proportional series g_m.

$$W_p^2 = \sum_{m=0}^{\infty} g_m \left(\frac{x}{R}\right)^{2m}, \qquad g_0 = W_{p\text{-axial}}^2. \tag{22}$$

This approach is suitable for electron density distributions that are commonly expected, such as the zero-order Bessel function for diffusion-dominated plasmas or the uniform distribution for recombination-dominated plasmas. The assumed distribution will be based on the experimenter's best estimate of the dominant processes in the plasma. For more complicated assumed distribution, attention would have to be paid to the convergence of the series.

It will sometimes be desirable to test a hypothesis about the distribution shape by observing whether measurements in several different modes (which sample different parts of the plasma most strongly) give consistent density measurements. Several different distributions can be tested to obtain maximal consistency. An example of this approach will be given later.

We next assume that in the plasma E may be expanded in powers of x. Substituting a power series for E in (20) we find the solution

$$E = \sum_{p=0}^{\infty} \frac{T_p}{R^{2p}} x^{2p+1} \tag{23}$$

$$H = -\frac{1}{jW\eta_0} \sum_{p=0}^{\infty} (2p+2) \frac{T_p}{R^{2p}} x^{2p} \tag{24}$$

where T_0 is arbitrary and

$$T_{p+1} = \frac{\left(\sum_{m=0}^{p} T_{p-m} g_m\right) - h_0^2 T_p}{4p^2 + 12p + 8}, \quad p = 0, 1, 2, \cdots. \tag{25}$$

(Note that T_p is denoted as $T(N)$ in the computer program.)

It should be mentioned in passing that the normalizing factor R^{2p} in (23) had to be inserted to eliminate an underflow problem. When the series for E was written as

$$E = \sum_{p=0}^{\infty} t_p x^{2p+1} \tag{26}$$

the t_p rapidly became too small for our computer to handle. At $x = R$, we equate the two expressions for E/H derived from (14), (15), and (23), (24). This eliminates the unknown constant F, and leads to the equation

$$c_4 \sum_{p=0}^{\infty} (2p+2) T_p = \sum_{p=0}^{\infty} T_p R \tag{27}$$

where

$$c_4 \equiv \frac{J_1(h_3R) + c_3Y_1(h_3R)}{h_3[J_0(h_3R) + c_3Y_0(h_3R)]}. \tag{28}$$

We manipulate (27) into a form convenient for numerical solution:

$$\text{ZFUNC} \equiv \sum_{p=0}^{\infty} T_p(2c_4(p+1) - R) = 0. \tag{29}$$

It may be observed from (25) that the T_p depend on the frequency parameter h_0 and on g_0, the axial value of W_p^2. The method of solution is to choose a frequency and then vary g_0 until ZFUNC = 0.

The procedure for TM_{0n0} modes is exactly parallel to the TE case just considered. The normalized equation to be solved is

$$\frac{d^2E}{dx^2} + \frac{1}{x}\frac{dE}{dx} + W^2n^2E = 0. \tag{30}$$

The series expansions for E and H in the plasma are

$$E = \sum_{p=0}^{\infty} \frac{T_p}{R^{2p-1}} x^{2p} \tag{31}$$

$$H = \frac{1}{j\eta_0 W} \sum_{p=0}^{\infty} 2p \frac{T_p}{R^{2p-1}} x^{2p-1}. \tag{32}$$

The computational problem to be solved is

$$\text{ZFUNC} \equiv \sum_{p=0}^{\infty} T_p[R - 2pk_4] = 0 \tag{33}$$

where

$$k_4 = -\frac{J_0(n_gWR) + k_3Y_0(n_gWR)}{n_gW[J_1(n_gWR) + k_3Y_1(n_gWR)]} \tag{34}$$

$$k_3 = \frac{k_2n_gJ_1(n_gWQ) - J_0(n_gWQ)}{Y_0(n_gWQ) - k_2N_gY_1(n_gWQ)} \tag{35}$$

$$k_2 = \frac{J_0(WQ) - k_1 Y_0(WQ)}{J_1(WQ) - k_1 Y_1(WQ)} \tag{36}$$

$$k_1 = \frac{J_0(Wp)}{Y_0(Wp)} \tag{37}$$

$$T_0 = \text{arbitrary}$$

$$T_{p+1} = \frac{\left(\sum_{m=0}^{p} g_m T_{p-m}\right) - W^2 T_p}{4(p+1)^2} R^2. \tag{38}$$

Note that although we have dealt only with TM_{0n0} modes, it would be straightforward to extend the calculation to deal with the more general TM_{mn0} case. We would anticipate

$$E = \hat{r}0 + \hat{\phi}0 + \hat{z}E(r)\cos m\phi$$

and would have, in place of (30),

$$\frac{d^2E}{dx^2} + \frac{1}{x}\frac{dE}{dx} + \left[W^2n^2 - \frac{m^2}{x^2}\right]E = 0.$$

III. The Programs

Two very similar programs have been written: TECAV to treat TE_{0np} cavity modes, and TMCAV to deal with TM_{0n0} modes. The program listings and the data card specifications appear in Part II. Some commentary on TECAV will be given here to make use and further development of the program easier. Essentially identical comments apply to TMCAV.

Input Data (Cards 240–580)

Real cavities differ in many respects from the ideal described mathematically above; there are holes for the glass tube to pass through, there are coupling loops or probes in the cavity, the walls are neither perfectly uniform nor perfectly conducting, etc. In order to make the mathematics approximate the behavior of the real cavity, calculations are carried out not for the precise dimensions of the real cavity, but rather for the slightly different "effective" dimensions of a mythical perfect cavity which matches the resonant frequencies of the real cavity under three specified conditions. *FWG* is the measured resonant frequency, in the absence of plasma, of the mode in which the cavity will be used for plasma measurements. *F*1 is the frequency of the same mode with the glass tube removed; and *F*2 is the frequency of any other identifiable TE_{0np} mode, also with the tube removed.

Note that the series d_m (called DDISTR in the program) which represents the assumed shape of the electron-density distribution, allows only even powers of (x/R). Thus the first term of the series multiplies $(x/R)^0$, the second, $(x/R)^2$, etc. This suffices for the representation of any physically possible distribution, because we can require $W_p^2(x) = W_p^2(-x)$ without in any way restricting the behavior of W_p^2 in the real-world regime $x > 0$. Note, too, the requirement that the series be normalized so that its first term is 1.0.

Effective Length and Radius of Cavity (Cards 600–650)

The resonant frequency of an empty TE_{0np} cavity of length l and radius a is

$$F = \frac{c}{2}\sqrt{\left(\frac{p}{l}\right)^2 + \left(\frac{J_{1n}}{\pi a}\right)^2} \tag{39}$$

where J_{1n} is the nth root of J_1. Given the frequencies *F*1 and *F*2 of two identified modes, we can therefore solve for effective values of l and a.

Print Input Data (Cards 670–860)

Check the printout to ensure that all data were correctly entered and that the effective length and radius are close to the real ones. If the effective values are far from the true ones, the mathematical model used is probably invalid for this cavity.

Compute Normalized Cavity Dimensions, Then Compute and Print Refractive Index of Glass (Cards 970–1230)

The program seeks the value of n_g which accounts for the shift in frequency from *F*1 to *FWG* when the glass tube is inserted in the cavity. This is done by using subroutine ROOT to find the value of n_g which makes ZFUNC = 0 under the assumptions $W = FWG/F1$ and $\omega_g^2 = 0$. For this one segment of the program it is convenient to set the normalization frequency ω_0 to $2\pi \cdot F1$. (For the remainder of the calculations, frequency will be normalized to *FWG*.) The printed result of the refractive index calculation should be close to the value usually measured for the variety of glass used. Typical microwave frequency refractive indices of glass are near 2.

Perturbation-Theory Solution (Cards 1330–1690)

A low-density asymptote is provided by perturbation theory [6] to check the exact calculation. A Simpson's rule integrator, SIMPQ, is used to evaluate

$$r_p = \frac{\int \frac{\omega_p^2}{\omega_0^2} E_0^2\, dv}{2\int \epsilon E_0^2\, dv} \tag{40}$$

with the temporary assumption $(\omega_{p-\text{axial}}/\omega_0)^2 = 1$. Then, for low densities,

$$\frac{\Delta\omega}{\omega_0} = r_p\left(\frac{\omega_{p-\text{axial}}}{\omega_0}\right)^2. \tag{41}$$

The fields are obtained by the same process of matching at boundaries used above for the exact calculation, except that a simple Bessel-function field appears in the central region.

$$E_0 = J_1(h_0 x), \qquad x < R \tag{42}$$

$$E_0 = c_5[J_1(h_3 x) + c_3 Y_1(h_3 x)], \qquad R \le x \le Q \tag{43}$$

$$E_0 = c_6[J_1(h_0 x) - c_1 Y_1(h_0 x)], \qquad Q \le x \le P \tag{44}$$

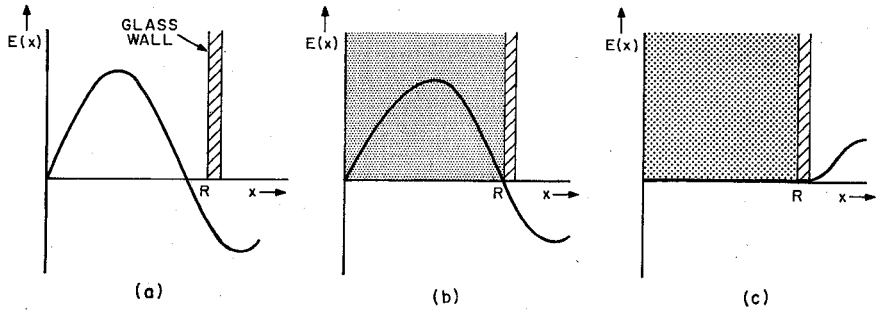

Fig. 2. Illustration of the way in which a high-order field distribution can cause an incorrect low value to be found for WMAX, the normalized resonant frequency at infinite electron density. Also either Fig. 2(a) or (b) illustrates an initial field distribution that will cause perturbation theory to predict too small a frequency shift for a given density. (a) No plasma. (b) $E(R)=0$. $W<$WMAX. (c) $E(R)=0$. $W=$WMAX.

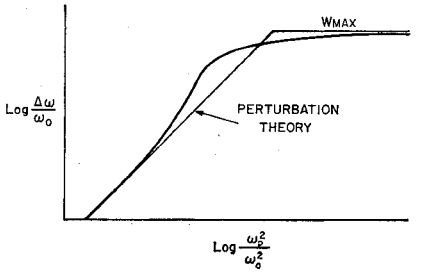

Fig. 3. Example of calibration curve which can be produced by initial field distribution such as that in Fig. 2(a) or (b). Note that perturbation theory predicts too small frequency shift for low densities.

where

$$c_5 = \frac{J_1(h_0R)}{J_0(h_3R) + c_3Y_1(h_3R)} \tag{45}$$

$$c_6 = c_5\frac{J_1(h_3Q) + c_3Y_1(h_3Q)}{J_1(h_0Q) - c_1Y_1(h_0Q)}. \tag{46}$$

Although the exact calculation usually approaches the perturbation-theory asymptote from below (as will be shown later), for high-order modes it may occasionally approach from above. Consider a cavity whose field distribution *without* plasma looks like Fig. 2(a). As the plasma density increases and forces the fields outward, the integral of ϵE^2 in the glass will decrease. Thus the denominator of (40), which uses the unperturbed field, will be too large, and the perturbation-theory value of $\Delta\omega$ will be smaller than the exact value. The resulting situation is shown in Fig. 3.

Main Loop (Cards 1770–2310)

Equation (29) is solved for $\omega_p{}^2{}_{-\text{axial}}/\omega_0{}^2$ at each of NINT uniformly spaced frequencies between *FWG* and FRANGE. The first frequency chosen is FREQ = *FWG* +(FRANGE–*FWG*)/NINT and the last is FREQ =FRANGE. If no root can be found, the calculation terminates. This condition will most often be due to the specified frequency shift exceeding the value that would result from infinite plasma density, or approaching it closely enough so that $(\omega_{p-\text{axial}}/\omega_0{}^2) > 1000$.

For each frequency specified, subroutine ROOT varies the normalized axial plasma frequency [g_0 in (22), called $G(1)$ in the program] until ZFUNC = 0. Subroutine ZEROTE is used to compute ZFUNC.

If K different plasma-distribution shapes have been specified by the input data, this root-finding procedure is carried out K times at each frequency.

Compute and Print WMAX (Cards 2330–2470)

As a check on the exact calculation of frequency shift versus plasma density this program segment calculates the frequency shift when the plasma is replaced by a perfectly conducting post. From (14), it can be seen that the condition $E(R)=0$ requires

$$J_1(h_3R) + c_3Y_1(h_3R) = 0. \tag{47}$$

Subroutine CCOMP calculates the value of the left side of (47) for any given W, and subroutine ROOT is used to vary W until, at the solution WMAX, the value comes out 0. WMAX should be the high-density asymptote of a plot of $(\omega_p{}^2/\omega_0{}^2)$ versus (ω/ω_0); this will be illustrated in Fig. 5.

Fig. 2 illustrates a difficulty which arises in this program segment when high-order modes are being considered. The boundary condition $E(R)=0$ can be met for frequencies substantially below WMAX; i.e., for noninfinite conductivities. To avoid these spurious solutions to (47) it is necessary to estimate rather closely the region in which the true root should be sought.

An upper limit to the region is obtained by treating the space between the plasma post and the cavity wall as a two-dimensional box whose resonances can be computed simply:

$$f_{np} = \frac{c}{2}\sqrt{\left(\frac{n}{w}\right)^2 + \left(\frac{\rho}{L}\right)^2} \tag{48}$$

where w is the width of the box (the distance from the plasma post to the cavity wall) and L its length (equal to the length l of the cylindrical cavity). If $N1$ is the radial order of the mode being studied and $P1$ its longitudinal order, the upper limit used will be $f_{(N1+1),P1}$.

The region's lower limit is taken as the highest fre-

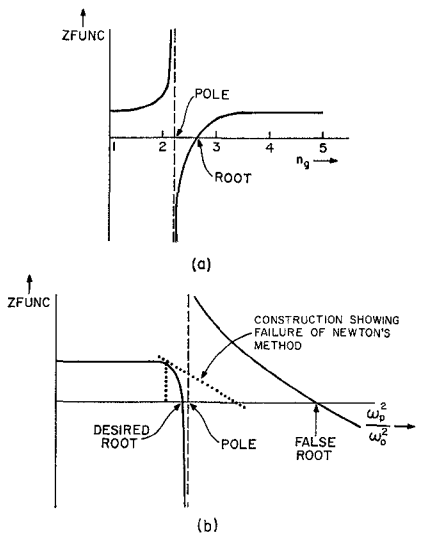

Fig. 4. Illustration of some disagreeable properties of ZFUNC.

quency for which the main loop of TECAV was able to find a corresponding electron density. If the control data supplied to TECAV specify a small value for FRANGE, this lower limit may not be stringent enough; a false root may occasionally be found, as illustrated in Fig. 2.

End-of-Program Routine (Cards 2490–2550)

After all requested data points have been computed, the program returns to its beginning to seek another set of data cards. This feature can be used to calibrate more than one cavity on a given computer run, to calculate data points for one given cavity with variable spacing (e.g., every 10 MHz for the first 200 MHz, then every 50 MHz for the first 1000 MHz), or to handle more than the allowed five different plasma-distribution shapes. If the program finds no additional data cards, it prints a message and stops.

Subroutine ROOT (Cards 2570–3650)

For any given function (computed by the arbitrary subroutine SUBR), ROOT seeks a value of the abscissa PARAM which reduces the absolute value of the function below a specified size. The routine begins by searching from BOTTOM to TOP for two values of PARAM between which the computed function changes sign; then homes in on the root by a binary search. The methods used are inelegant and rather slow, but they generally work despite the inhumane behavior of ZFUNC.

To understand the difficulties which this routine faces, consider the sketches in Fig. 4, which illustrate that the root of ZFUNC is often preceded by a pole. To a routine which simply looks for a sign change between two values of the abscissa, a simple pole and a root are indistinguishable. ROOT therefore tests successive ordinate values near a supposed root (cards 3380–3410) and rejects as poles the cases in which the ordinate increases in magnitude as the "root" is approached. If a pole is found, the subroutine makes one more attempt to find a true root before giving up (cards 3430–3600).

The first problem illustrated by Fig. 4(b) is that the true root of ZFUNC often lies very close to a pole. If the initial search for two abscissas, between which ZFUNC changes sign, is conducted by stepping in large intervals from BOTTOM to TOP, the sign change at the desired root can be missed entirely and the program winds up locating the false root instead. The 64-point initial search pattern used in TECAV's subroutine ROOT (cards 2810–2900) usually suffices to avoid this difficulty. At large frequency shifts or for high-order modes, the routine does occasionally fail.

To cope with this problem, we have provided in TMCAV an alternate, interchangeable version of ROOT (cards TM 2220–3010) which conducts its initial search for a sign change by scanning from BOTTOM to TOP in 4096 steps. A scan this small is time consuming (total program time typically goes up by a factor of 2 to 4), but very rarely misses a root.

A false root can generally be detected in the output data by a discontinuous jump in a plot of log (ω_p^2/ω_0^2) versus log $(\Delta\omega/\omega_0)$, or a failure of the plot to approach the perturbation-theory asymptote at small $\Delta\omega$.

Once a root has been isolated it is refined by binary search (cards 3210–3360). The dotted line in Fig. 4(b) illustrates why more sophisticated techniques fail (in this case Newton's method); an attempt to approximate the true root by fitting a tangent or a low-order polynomial to a known segment of ZFUNC will often cause a jump onto the wrong branch of the function. Methods which avoid this jump by using starting values that bracket the root generally seem to converge more slowly than the binary search. We attribute this to the very rapid approach of ZFUNC to zero when a pole is nearby.

The variable *IER* is used by ROOT to signal the main program if no root is found. The value of *IER* is then printed out by the main program. The most frequent usage is the statement "$IER=1$" which appears in the output list when the value of (ω_p^2/ω_0^2) exceeds 1000, and is therefore outside the range being searched. Cards 2640–2680 detail the possible values of *IER*.

Subroutine ZEROTE (Cards 3670–4260)

This routine computes ZFUNC according to (29). Enough terms of the infinite series are kept so that the last two terms retained each contribute less than one part in 100 000 to ZFUNC. Several hundred terms may be required for large frequency shifts and high-order modes. Double-precision arithmetic must be used to avoid intolerable roundoff error in such a long computation. Generally, of course, 15 or 20 terms of the series are entirely adequate.

Since the amplitude of E is arbitrary in the calculation of resonant frequency, the value of T_0 is arbitrary.

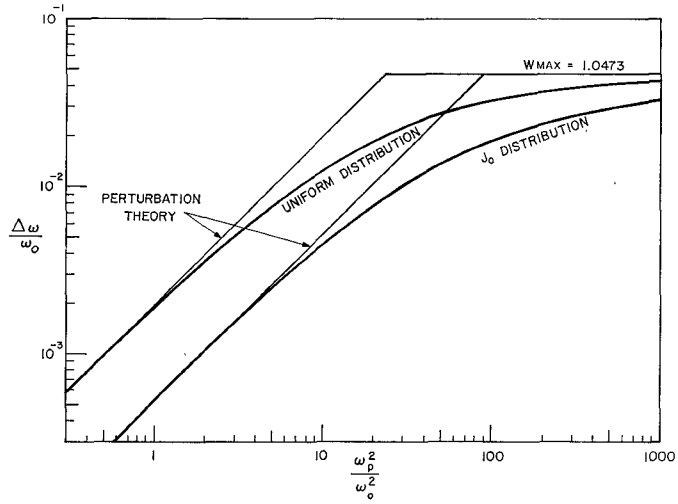

Fig. 5. Calibration curve for a typical TE_{011} cavity. Parameters of the cavity and values of the power-series coefficients used to represent the radial density variation are given in the data card specifications. Points on curve are from the sample output.

The value of 10^{-30} has been selected to minimize the number of occasions of computer overflow during the calculation of the T_p. If for a particular rare cavity either underflow or overflow occurs, the values of the T_p may be scaled by adjusting T_0 (card 3840).

Note, in comparing the computer programs to the mathematical derivations above, that Fortran's peculiarities require our designating T_0 as $T(1)$ in the program.

Function BESSEL (Cards 4670–5870)

Because TECAV spends a lot of time computing Bessel functions, it proved worthwhile to write a customized routine instead of using IBM's general-purpose library routine. The chief virtue of this subprogram is that it does no unnecessary work when called upon for several types of Bessel functions of the same argument. Its accuracy is on the order of one part in 10^9.

Subroutine SIMPQ (Cards 5890–6220)

This routine integrates any given function by Simpson's rule using a progressively finer grid of data points until two successive computations differ by less than one part in 10^6. If the integration has not reached this accuracy by the time a 2048 point grid is used, the routine gives up, returns its latest computed approximation to the integral, and sets an error signal.

IV. Examples and Applications

Fig. 5 shows the output of a computer run for a particular TE_{011} cavity. For this run we set FRANGE = 9698.5 MHz and NINT = 50 MHz. Observe that the exact calculation does approach the asymptotes provided by WMAX and perturbation theory. The job took 29 s of real time to run on the University of Illinois' time-shared IBM 360/75, and cost 2.75 dollars. To get this short operating time, it was essential to use an efficient compiler (in this case IBM's Fortran H, option 2, level 18) to prepare the object deck used, even at the price of long compilation time. The importance of an efficient object program becomes extremely clear for high-order modes and large frequency shifts, which can require several minutes to calculate 50 data points.

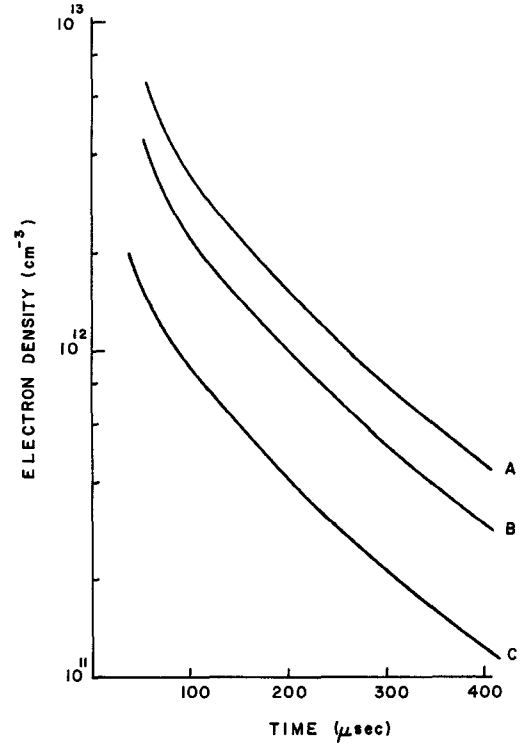

Fig. 6. Electron density decay in an afterglow plasma in 10-torr neon. *A* and *B*—TE and TM cavity data, respectively, assuming a diffusion distribution. *C*—TE and TM cavity data assuming a recombination distribution.

As shown in Fig. 5, calibration curves were generated for two assumed electron-density distributions. If this procedure is repeated for different cavity modes, then by comparing the experimental frequency shifts observed on different modes with the calibration curves, one can, within reason, obtain a very good indication of the plasma distribution. An example of this is shown in Fig. 6 [9].

In this particular experiment it was desired to find the form of the plasma distribution in a decaying afterglow produced in 10-torr neon. Frequency shifts, as a function of time in the afterglow were recorded for TM_{010} and TE_{011} cavities, and the axial electron density was calculated from the calibration curves for two different assumed distributions: the J_0 (diffusion-controlled) and the uniform (recombination-controlled) distributions. As can be seen from Fig. 6, excellent agreement was obtained for an assumed uniform distribution, which indicated that this plasma was recombination controlled, as expected.

If the plasma distribution is reasonably well behaved, then this approach is convenient and effective. A similar approach has been examined by Kent *et al.* [10]. If, however, the plasma is doing strange things, this technique would not work well. In general, of course, if the

frequency shifts are known for a large number of cavity modes, it would be possible to invert the data (similar to Abel inversions) to obtain the distribution. This technique is difficult to apply, however, and requires some sophisticated analysis.

V. Collisions

The programs described above assume a lossless cavity and a collisionless plasma, approximations which have thus far been adequate for our needs. If it proves desirable to take collisions into account, it should be straightforward to do this by using the definition of Q.

$$Q = 2\pi \frac{\text{total energy stored in cavity}}{\text{energy lost per period}} \tag{49}$$

or

$$Q = \frac{2\omega \int \epsilon E^2 \, dv}{\int \sigma E^2 \, dv} . \tag{50}$$

If we use the Lorentz formula for the conductivity of a plasma (Shkarofsky shows that the Lorentz formula can be doctored to give useful results even if ν depends on velocity [11]), (50) leads to the formula

$$Q = \frac{2\omega \int \epsilon E^2 \, dv}{\int \frac{\nu_m}{\nu_m^2 + \omega^2} \epsilon_0 \omega_p^2 E^2 \, dv} . \tag{51}$$

The appropriate fields to use here are not the unperturbed fields, but rather the "exact" fields available in ZEROTE (or ZEROTM) as the series T_p. Spatial variation of ν_m and ω_p^2 can easily be taken into account since the integral would be performed numerically in any event.

Several points must be argued to justify this approach. First, the addition of collisions must not result in fields very different from the collisionless approximation. This is probably a reasonable assumption so long as $(\nu/\omega)^2 < 0.1$. Second, we know that in the high-density regime where these programs are most useful, the cavity fields are significantly perturbed, which will change the cavity losses due to wall resistivity and stray radiation. However, a few sample calculations will show that whenever densities are high enough to force a typical cavity out of the perturbation-theory regime, the plasma losses will generally be high enough to produce large changes in Q and entirely mask other loss effects. Third, it must be emphasized that (51) predicts *unloaded* Q. The effects of loading by the circuits coupled to the cavity may change when high-density plasmas perturb the fields. Changes in coupling must be observed in order to correctly deduce unloaded Q under dynamic conditions.

We offer, finally, a speculation about a simple but unproven method of dealing with collisions. The perturbation-theory formula for Q corresponding to (40) and (41), assuming collision frequency ν_m to be position independent, is [6]

$$\Delta\left(\frac{1}{Q}\right) = \frac{\nu_m/\omega}{\omega^2 + \nu_m^2} \frac{\int \epsilon_0 \omega_p^2 E_0^2 \, dv}{\int \epsilon E_0^2 \, dv} . \tag{52}$$

Combining this with (40) and (41) gives

$$\Delta\left(\frac{1}{Q}\right) = -2 \frac{\nu_m}{\omega} \frac{\Delta\omega}{\omega_0} \tag{53}$$

so that ν_m can be obtained from measurements of frequency and Q *without evaluating any integrals*. We speculate that perhaps (53) or an equally simple formula may continue to hold at high densities even though neither $\Delta\omega$ nor $\Delta(1/(Q)$ may be obtained from the perturbation formulas. This would make it possible to compute collision frequency with no recourse to numerical integration, even at high densities.

VI. Conclusions

A description and listing are given for computer programs that provide efficient accurate calibration curves for microwave cavities used in plasma diagnostics. The program is based upon the exact solution of Maxwell's equations, and so can take into account the effect of the discharge tube and can provide accurate plots of resonant frequency versus plasma density for a range from zero to essentially infinite electron density. These plots can be made for fairly arbitrary dimensions of the cylindrical cavity used and for a large variety of possible cavity modes, as well as for a large variety of possible plasma profiles within the discharge tube.

Although the computer program gives accurate results, some remarks are in order regarding the care that must be taken in obtaining and interpreting the experimental results, as well as some of the common problems that occur in the use of this technique. First of all, the accuracy in determining the plasma density depends greatly on the accuracy in determining the resonant frequency of the cavity. For this reason it is essential that the cavity Q be as high as possible and the discharge tube be made of low-loss glass (quartz or 7070 Pyrex). The effect of small errors in the frequency shift can be especially severe for large plasma densities, as can be clearly seen in Fig. 5. Another problem that occurs at large electron densities is that this is also quite often the region of high electron-collision frequency (electron–ion as well as electron–neutral). This decreases the Q of the cavity, broadens the resonance, and makes the determination of the exact resonant frequency difficult. In fact, if the collision frequency is high, the resonances may be completely washed out. Needless to say, this

also suggests that considerable care must be taken in coupling the cavity to the measurement system. A tradeoff will have to be made to keep the coupling as loose as possible to preserve the high Q while retaining sufficient coupling to obtain a readable signal.

Microwave cavity techniques have been used widely in pulsed (decaying afterglow) plasma studies where the plasmas are usually quiet and well-behaved. If a plot of density versus time in the afterglow is to be obtained, then it is necessary that the plasma conditions be repeatable from pulse to pulse. In dc discharges many more problems arise. Due to the high electron temperatures, the collision frequencies in such discharges are usually large and can wash out the cavity resonances. Furthermore, the fluctuations, striations, etc., that are commonly found in dc discharges, as well as the microwave radiation directly into the cavity and the possible excitation and interaction of plasma modes, can contribute an excessive amount of noise to the detector signal and can make meaningful measurements impossible. Under such circumstances, it is sometimes possible to crowbar off the discharge for a short period of time, make measurements in the afterglow, and extrapolate back to the switch-off time to obtain estimates of the plasma density.

References

[1] S. C. Brown *et al.*, Res. Lab. Electron., Mass. Inst. Technol., Cambridge, Mass., Tech. Rep. 66, 1948.

[2] S. C. Brown and D. J. Rose, "Methods of measuring the properties of ionized gases at high frequencies—Part I: Measurements of Q," *J. Appl. Phys.*, vol. 23, p. 711, 1952.
——, "Methods of measuring the properties of ionized gases at high frequencies—Part II: Measurement of electric field," *ibid.*, vol. 23, p. 719.
——, "Methods of measuring the properties of ionized gases at high frequencies—Part III: Measurement of discharge admittance and electron density," *ibid.*, vol. 23, p. 1028.

[3] L. Gould and S. C. Brown, "Methods of measuring the properties of ionized gases at high frequencies—Part IV: A null method of measuring the discharge admittance," *J. Appl. Phys.*, vol. 24, p. 1053, 1953.

[4] H. A. Blevins and J. A. Reynolds, "Resonances TE_{0mn}, TM_{1m0}) of a cylindrical cavity containing a nonuniform plasma column," *J. Appl. Phys.*, vol. 40, p. 3899, 1969.

[5] J. L. Shohet and A. J. Hatch, "Eigenvalues of a microwave cavity filled with a plasma of variable radial density," *J. Appl. Phys.*, vol. 41, p. 2610, 1970.

[6] J. C. Ingraham and S. C. Brown, Res. Lab. Electron., Mass. Inst. Technol., Cambridge, Mass., Tech. Rep. 454, 1966 (available from CFSTI as AD645110).

[7] K. I. Thomassen, "Microwave plasma density measurements," *J. Appl. Phys.*, vol. 36, p. 3642, 1965.

[8] S. Ramo, J. R. Whinnery, and T. VanDuzer, *Fields and Waves in Communications Electronics*. New York: Wiley, 1965.

[9] E. E. Wisniewski, private communication.

[10] G. Kent, D. Sinnott, and P. Kent, "Plasma electron density distribution from cavity frequency shift data," *J. Appl. Phys.*, vol. 42, p. 2849, 1971.

[11] I. P. Shkarofsky, "Values of the transport coefficients in a plasma for any degree of ionization based on a Maxwellian distribution," *Can. J. Phys.*, vol. 39, p. 1619, 1961.

Automatic Digital Method for Measuring the Permittivity of Thin Dielectric Films

MARIA A. RZEPECKA, MEMBER, IEEE, AND M. A. K. HAMID, SENIOR MEMBER, IEEE

Abstract—**One of the most promising techniques for measuring the electric permittivity at microwave frequencies of thin dielectric materials of the order of 0.1 to 10 μm, is the cavity perturbation method. For thin films of this type, it is necessary to determine accurately and display small changes in the resonant frequency and Q factor of the cavity in the presence of the material sample.**

A circuit for the simultaneous measurement and digital readout of the resonant frequency and Q factor of microwave cavity is described. For the resonant frequency measurement, a very efficient automatic frequency circuit, with a homodyne modulation-detection bridge and frequency stabilization loop, is applied. Theoretical analysis and experimental results with this circuit show that an accuracy of 5×10^{-7} can be achieved in the resonant frequency measurement.

For measuring the Q factor, two similar circuits are described. The technique is based on measuring the phase shift of the envelope of an amplitude modulated microwave signal when this signal is transmitted through a resonant cavity at resonance. Although an accuracy of 0.5 percent in the Q factor can be achieved, it is shown that the main limiting factor in both circuits is the accuracy of phase shift determination at RF frequencies.

Manuscript received March 1, 1971; revised July 13, 1971.

The authors are with the Department of Electrical Engineering, University of Manitoba, Winnipeg, Canada. This work was supported in part by the National Research Council of Canada, under Grants A-3326 and A-7240, in part by the Defence Research Board of Canada, under Grants 6801-37 and 3801-42, and in part by the Faculty of Graduate Studies, University of Manitoba.

I. Introduction

THE permittivity of thin dielectric films has been of increasing interest due to its importance in the properties of semiconductor thin films and integrated circuits at microwave frequencies. More recently, the properties of thin biological films have received con-